Optical studies of charged excitons in II–VI semiconductor quantum wells

2003 J. Phys.: Condens. Matter 15 R471

(http://iopscience.iop.org/0953-8984/15/13/201)

INSTITUTE OF PHYSICS PUBLISHING JOURNAL OF PHYSICS: CONDENSED MATTER

J. Phys.: Condens. Matter **15** (2003) R471–R493 PII: S0953-8984(03)39620-1

TOPICAL REVIEW

Optical studies of charged excitons in II–VI semiconductor quantum wells

P Kossacki

Institute of Experimental Physics, Warsaw University, Hóza 69, 00-681 Warsaw, Poland

Received 11 February 2003
Published 24 March 2003
Online at stacks.iop.org/JPhysCM/15/R471

Abstract

A brief review is given of optical studies of doped II–VI quantum wells. The properties of exciton states, neutral as well as positively and negatively charged, are discussed. A wide range of optical measurements is presented: CW as well as picosecond and femtosecond time-resolved absorption, photoluminescence (PL) and PL excitation. The experiments were performed at various carrier concentrations ($>10^{11}$ cm^{-2}) and temperatures (up to a few tens of kelvins). This review is limited to zero or low magnetic fields, used only to polarize spins of carriers. We discuss the obtained values of various fundamental parameters of the excitonic states: energies, optical transition probabilities and characteristic times of their formation, thermalization and decay.

Contents

0953-8984/03/130471+23$30.00

1. Introduction

1.1. Historical background

The existence of charged excitons in semiconductors was predicted long ago (1958) by Lampert [1]. He found that an additional carrier (electron or hole) can interact with an exciton forming a singly charged three-particle complex named later a charged exciton or trion. Both positively (X^+) and negatively (X^-) charged excitons were predicted. However, the small binding energy of the additional carrier makes the observation of the charged excitons in bulk materials very difficult and only possible in extremely pure crystals [2, 3]. In 2D structures the binding energy is strongly enhanced and often charged excitons dominate the optical spectra of semiconductor quantum wells containing 2D carrier gas. The first identification of charged excitons in a 2D structure was done by Kheng *et al* [4], who observed an optical transition at an energy a few millielectronvolts below the free (neutral) exciton line in modulation n-doped CdTe/CdZnTe quantum wells. They were able to produce convincing arguments in favour of the negatively charged exciton origin of the observed transition. Their result was rapidly followed by experimental evidence for both kinds of exciton in III–V and II–VI 2D systems [5–9]. Since then properties of such complexes have been intensively studied, primarily by means of spectroscopic techniques. In fact, a number of earlier experimental observations, interpreted as impurity or defect related transitions, can be viewed today as being due to charged excitons. After the first controversy related to proper identification of the charged excitons, several important questions related to their properties were addressed. For example, detailed studies were performed on the selection rules [10, 30, 63], dynamics [5, 11, 16], role of the carrier gas localization [12–14], localization of a charged exciton in a QW [14–16, 19, 43, 73], the stability of the complex in high magnetic field [17, 18] and interaction between neutral and charged exciton states [19, 20]. The properties of charged excitons in the quantum-Hall-effect regime were also studied [10, 18, 56, 57].

We wish to discuss here selected problems related to optical properties of charged excitons. They will be illustrated by experimental results obtained on modulation doped CdTe-based quantum wells. Creation of charged exciton states directly by light in the absorption process will be considered and photon energy as well as oscillator strength of the corresponding absorption line will be analysed. We also plan to present a complete description of charged exciton dynamics. The formation time dependence on carrier concentration will be discussed as well as the decay of trion photoluminescence (PL). We will discuss the variation of radiative lifetime of the charged exciton with temperature and carrier concentration. It will be demonstrated that the experimentally observed linear increase of lifetime with temperature is predicted for delocalized trions for which the radiative recombination can take place with a specific strongly k-dependent selection rule [21, 22]. The same model describes correctly the change of PL line shape with temperature as well as the variation of absorption and PL spectra with carrier concentration. We will also discuss examples of phenomena going beyond the simple picture.

1.2. Samples

The samples which permit observation of charged excitons are heterostructures with quantum wells containing pre-existing carriers. The well width and heterostructure material determine

the energy distance between neutral and charged excitons. The materials with larger neutral exciton binding energy are more convenient for studies of charged excitons. Most of the studies presented here were done on modulation-doped CdTe-based quantum wells. Such a choice was motivated by the good structural and spectroscopic quality, comparable to that of equivalent GaAs-based samples [5, 6], accompanied by much larger dissociation energies. The samples containing a single 8 or 10 nm wide CdTe or $Cd_{1-x}Mn_xTe$ QW were grown by molecular beam epitaxy.

The necessary carrier gas concentration in the quantum well was obtained using several methods: by modulation doping, optical excitation [53] or from surface states [52]. As an example two different designs are presented. They were used for observation of positively and negatively charged excitons respectively. In the first case the barriers were made of $Cd_{1-y-z}Mg_yZn_zTe$, in which the Mg content ($y = 0.25$–0.28) determined the valence band offset, while the presence of Zn ($z = 0.08$–0.07) ensured a good lattice match to the $Cd_{0.88}Zn_{0.12}Te$ substrate. The barriers were doped by nitrogen at a distance 20 nm from the QW on the surface side. Such a design makes it possible to tune the hole concentration isothermally by varying the intensity of illumination with photons of energy greater than the bandgap of the barrier material [23]. It was possible to tune the hole concentration in the range from 1.3×10^{10} to 1.6×10^{11} cm^{-2}.

The samples used for X^- observation were one-side modulation-doped CdTe/$Cd_{0.75}Mg_{0.25}$Te or $Cd_{1-x}Mn_xTe/Cd_{0.75}Mg_{0.25}Te$ heterostructures. The remote donor layer of iodine was located 10 nm from the QW. Its thickness was changed in steps within the same sample. This allowed us to tune the density of the electron gas in steps by selecting a spot on the sample surface. Additionally, on a given spot, the electron density could be increased further by illuminating the sample with light of energy higher than the energy gap of the barrier. The mechanism of this effect is based on the competition between the QW and surface states [35] which can both trap carriers, and is similar to one used in p-type samples. The maximum attainable electron density was 2×10^{11} cm^{-2}.

A particular group of samples are heterostructures without intentional doping. The first observed trion lines were found in MBE grown CdTe/CdZnTe heterostructures in which the barrier material is naturally n-type [4]. Similarly quantum wells with CdMgTe barriers are often p-type because of surface states which act as acceptor centres [35].

1.3. Experimental details

Many different spectroscopic methods may be used in studies of charged excitons. The most straightforward techniques are CW transmission, reflectivity and PL measurements. They were extensively used in studies versus temperature or magnetic field (see for example [4–9, 23]), but more complex techniques were also applied in many cases. For example time resolved experiments were done in both PL and pump and probe configurations [11, 12, 22, 27, 28, 34]. The charged exciton properties were also investigated by the four-wave mixing technique [15, 19, 58] or near field spectroscopy [13]. More complex heterostructures were also exploited such as microcavities [20] used in oscillator strength studies and diode structures used to tune carrier gas concentration [54]. Most of the results presented here were obtained in two standard magneto-optic set-ups. The experiments were carried out in helium cryostats equipped with superconducting magnets. PL was excited by Al_2O_3:Ti lasers, with an intensity less than 2 mW cm^{-2} in CW experiments, or by a picosecond tuneable Al_2O_3:Ti laser with a 2 ps pulse width, a repetition rate of 80 MHz and an averaged power density of less than 100 mW cm^{-2} in time-resolved ones. The signal was collected through a spectrometer by a CCD camera or a 2D streak camera with 10 ps resolution. The

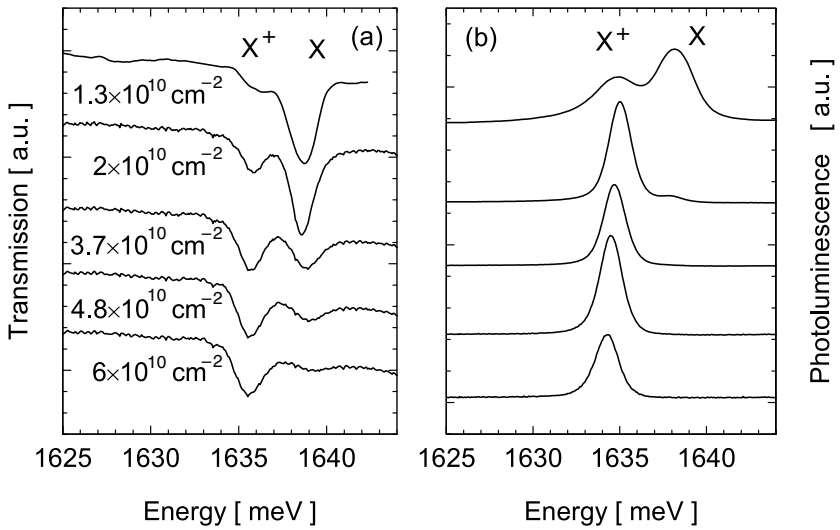

Figure 1. Absorption (a) and PL (b) spectra of an 8 nm wide $Cd_{0.998}Mn_{0.002}Te$ quantum well with $Cd_{0.66}Mg_{0.27}Zn_{0.07}Te$ barriers at indicated concentrations of 2D hole gas (data from [23]).

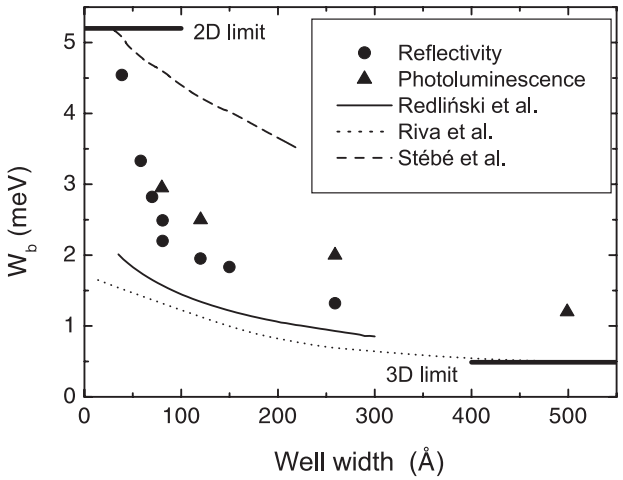

Figure 2. Dissociation energy of negatively charged exciton as a function of the CdTe/$Cd_{1-y}Mg_yTe$ quantum well width. Points represent experimental data; curves were taken from numerical simulation by Riva *et al* [60], Stébé *et al* [61] and Redliński and Kossut [59] (graph from [62]).

pump and probe experiments were done with a 40 fs tuneable Al_2O_3:Ti laser. An additional illumination, serving to change the hole or electron density, was produced by standard halogen lamps equipped with one blue and several grey filters.

This review is limited to experiments without magnetic field or in a weak field used only to control the spin polarization of the carriers. Stronger fields significantly modify the electronic wavefunctions and lead to many fascinating effects resulting from Landau quantization such as the quantum Hall effect and accompanying optical properties, which would require separate attention.

2. Charged exciton optical transition

2.1. Transition energy

Transitions related to charged excitons are observed in both absorption and PL experiments. They are seen as narrow lines below the energy of a neutral exciton (see figure 1). The distance between the neutral and charged excitons (dissociation energy) depends on the semiconductor material, but for bulk crystals it is typically only a few per cent of the neutral exciton binding energy [1]. It is usually too small to make the charged exciton line sufficiently resolved for experimental observation. Confinement in a quantum well enhances both neutral exciton (X) binding energy and charged exciton dissociation energy. Similarly to X binding energy, dissociation energy varies with QW width and increases significantly with confinement of the carriers. In different samples the dissociation energy varies from less than 1 to above 10 meV but always remains smaller than the binding energy of a neutral exciton to a neutral donor (D ^{0}X) or acceptor (A ^{0}X) in the same quantum well. For example in an 80 Å quantum well of CdTe with CdZnTe barriers these energies are approximately 2, 2 and 4 meV for X^-, X^+ and D ^{0}X respectively [4]. The example dependence of X^- dissociation energy versus QW width in CdTe/$Cd_{1-y}Mg_yTe$ quantum wells is presented in figure 2. Similar dependence was obtained for different materials such as ZnSe and both kinds of charged exciton: positively and negatively charged [39, 59, 62]. The experimental values usually agree pretty well with theoretical predictions which were made by many authors [21, 25, 59–61]. However, comparing experimental and theoretical data has to be done with some attention. Most theoretical models consider the charged exciton as a three-particle complex (two holes and one electron—X^+—or two electrons and one hole—X^-). In a real experiment we deal with nonzero carrier concentration. Actually, it was shown that dissociation energy increases with carrier gas concentration. This leads to dispersion of experimental data. Correctly, one should compare the experimental value extrapolated to zero carrier concentration with the theoretical one.

The dependence of dissociation energy on background carrier concentration was observed and studied in many absorption experiments without and with magnetic field. The increase was found to be linear with Fermi energy of the degenerate carrier gas. This effect is common to positively [23] and negatively charged excitons [37], as well as for different materials [38, 39]. This observation might be explained in a simple intuitive picture: both the neutral exciton and the charged exciton are due to the existence of a bound level which appears in the 2D gas in the presence of a carrier of opposite sign (i.e., of a hole in the case of an electron gas, or of an electron in the case of a hole gas). The neutral exciton then corresponds to a single occupancy of this level. The charged exciton involves, in addition to the creation of the exciton, the transfer of a carrier of opposite spin from the Fermi level down to the bound level. If we assume that the binding energy of both states is the same, we obtain that the X–X^+ (X–X^-) splitting exhibits, in addition to the binding energy, an energy equal to the Fermi energy. A similar effect was predicted by Hawrylak [40] for high concentration of electron gas and dispersionless holes.

A more accurate calculation still remains a challenge [41]. Nevertheless, several aspects of the experimental findings can be explained. For example, it was shown that the dissociation energy is a linear function of the concentration in only one hole spin subband (the one with the spin opposite to that of the photocreated hole) (see figure 3(a)) [23].

The slope of the linear dependence is significantly different from the predicted value of unity. It varies from 1.7 for X^+ to slightly above unity for X^- in a CdTe-based QW, but a value as high as ∼6 was reported for GaAs QW [38]. This goes beyond a simple-minded picture. Also, the temperature dependence needs a correct theoretical explanation. It was found that

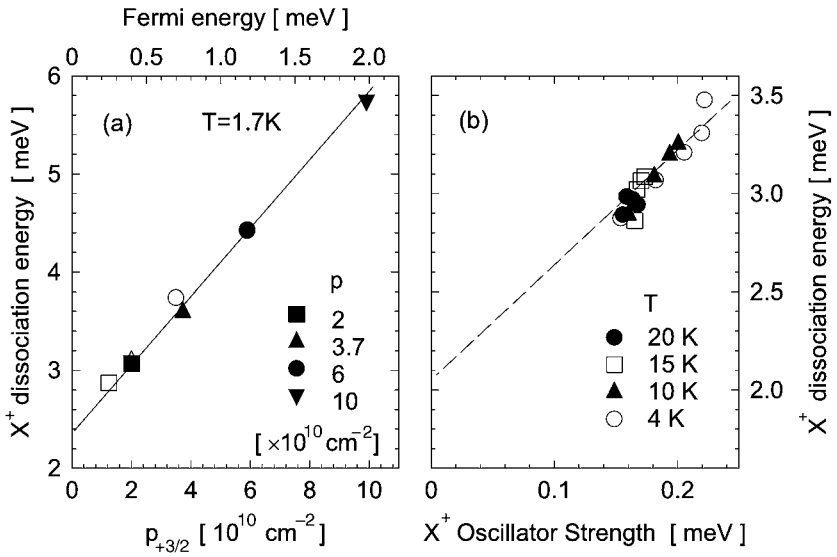

Figure 3. (a) Dissociation energy of X^+ as a function of the hole gas concentration in the spin subband promoting the X^+ formation (full symbols, complete spin polarization of holes; open symbols, no applied field). (b) Dissociation energy of X^+ as a function of the X^+ oscillator strength for different temperatures. Data obtained for an 8 nm wide $Cd_{0.998}Mn_{0.002}Te$ quantum well with $Cd_{0.66}Mg_{0.27}Zn_{0.07}Te$ barriers (graph from proceedings of *ICPS 2002* [68]).

the dissociation energy is decreasing with increasing temperature, as one could expect when hole gas degeneracy is broken. This dependence was found to be proportional to the variation of the X^+ oscillator strength (figure 3(b)).

2.2. Line intensity in absorption

Transitions related to formation of charged excitons are observed in both absorption and PL experiments. The example spectra for different carrier gas concentrations are presented in figure 1 [23]. The relative intensity of both lines depends strongly on carrier gas concentration and temperature. The neutral exciton dominates both kinds of spectrum for the lowest concentrations. When the carrier concentration increases, the low-energy (trion) line becomes more intense while the other one weakens and finally disappears. The limit for neutral exciton observation is different for absorption and PL experiments. For holes it is about 6×10^{10} and 2×10^{10} cm^{-2} respectively. The intensity of the PL line will be discussed in the next chapter. In transmission the presence of carriers attenuates the neutral exciton line, due to screening and phase-space filling. Simultaneously, the presence of carriers, necessary for creation of charged excitons, enhances the X^+ or X^- line with respect to the X line. For low carrier concentration, the intensity of the X^+ or X^- line is proportional to the concentration [4, 30]. In higher carrier gas concentrations the intensity starts to saturate due to filling of states with higher k-vectors. This initial proportionality may be used to identify the charged exciton transition but the precise knowledge of carrier concentration is needed. This is not always easy to determine. For example the complex processes related to depopulation or creation of carrier gas in a quantum well may give misleading results. If carrier population is linearly increased by laser illumination one observes a quadratic increase of trion PL intensity versus excitation power. This might even be interpreted erroneously as a fingerprint of a biexciton.

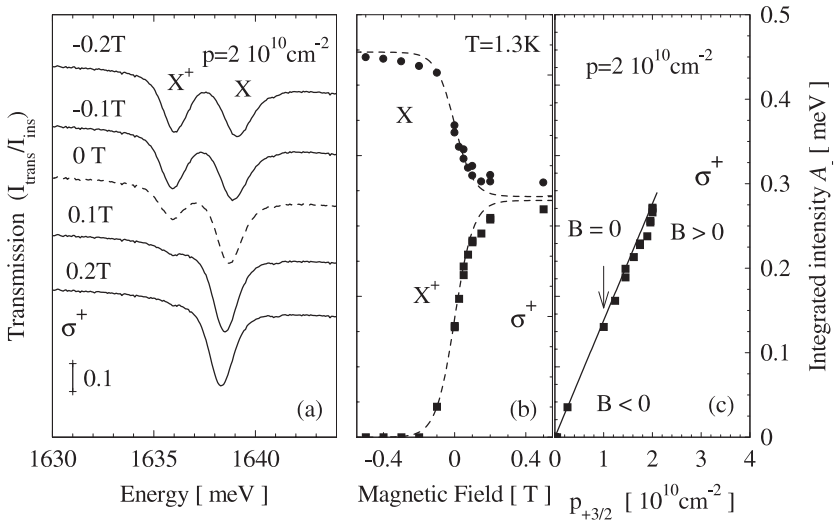

Figure 4. Transmission of an 8 nm wide $Cd_{0.998}Mn_{0.002}Te$ quantum well with $Cd_{0.66}Mg_{0.27}Zn_{0.07}Te$ barriers in magnetic field, obtained for low hole gas concentration ($p = 2 \times 10^{10}$ cm^{-2}) at a temperature of 1.3 K: spectra (a), integrated line intensities as a function of magnetic field (b) and the hole gas concentration in the spin subband promoting the X^+ formation (c) (data from [23]).

The proper identification of the trion line might be based on the selection rules of absorption in magnetic field. The fundamental state of the charged exciton (in zero and low magnetic field) is a singlet. Therefore the photo-created carrier has to be of opposite spin than the pre-existing one. The defined spin of a pre-existing carrier determines the circular polarization of the absorbed photon. Particularly, this is the case of an experiment in magnetic field when the carrier gas is spin polarized. Then the absorption line can only be observed in one circular polarization. The necessary condition for such a simple selection rule is a sufficiently large g-factor (larger than Landau splitting). This condition is particularly easy to fulfil in semimagnetic semiconductors where giant Zeeman splitting enhances the g-factor up to thousands [52].

Figure 4(a) shows transmission spectra at a low hole concentration, taken at several magnetic fields in both circular polarizations. We observe a characteristic population effect on the low-energy line: its intensity increases with field in the σ^- polarization, while it decreases in σ^+. At a field of about 0.3 T, the σ^+ component disappears completely. In σ^+ polarization, the creation of a X^+ exciton in its singlet state involves a photocreated spin-up hole and a pre-existing spin-down hole. Thus, this observation reflects the absence of such spin-down holes. Note, however, that in a $Cd_{1-x}Mn_xTe$ quantum well, in contrast to a CdTe one, the giant Zeeman effect in the conduction band leads to the same sign of circular dichroism for the negatively charged exciton.

However, g-factors of electrons and holes are different in most cases. This might be used for an unambiguous identification of the sign of the charged exciton. In the case of CdMnTe material the giant Zeeman splitting is four times larger in the valence band than in the conduction band. An example quantitative test was done for the X^+ transition [23]. First, we fit the measured exciton splitting using the phenomenological expressions given in [51] for bulk material, using the exact Mn content x as adjustable parameter and assuming that the temperature of the Mn spins T_S may be slightly higher. A good fit is obtained for $x = 0.0018$.

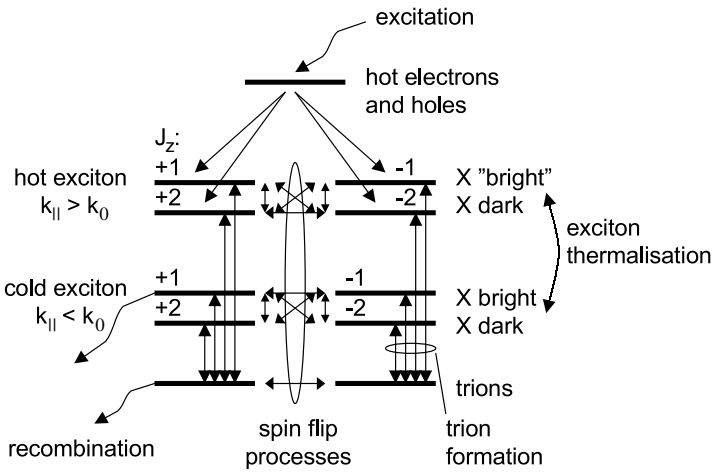

Figure 5. Schematic representation of the complete relaxation diagram, including relevant energy levels and processes.

We then analyse the intensity of both transitions by fitting two Gaussian functions to the absorption spectra. The integrated intensity of respective lines is represented versus magnetic field in figure 4(b). At constant total hole concentration p, we expect the intensity of the X^+ line to be roughly proportional to the population of holes with the appropriate spin, i.e., $S_z = +3/2$ in σ^+ polarization, respectively. Using a Maxwell–Boltzmann distribution between the Zeeman-split subbands to describe the hole concentration, we obtain for the intensity

$$A_{\pm}(\Delta) = A(\infty)\frac{1}{1+\exp(\mp\Delta/k_BT)} \tag{1}$$

where Δ denotes the valence-band Zeeman splitting and is taken to be positive for one spin and negative for the other one, T is the carrier gas temperature and k_B is the Boltzmann constant. $A(\infty)$ is the maximum intensity, achieved at total hole spin polarization. Indices + and − of the intensity denote the two circular polarizations of light. To calculate the intensity, we assume for the conduction-to-valence-band splitting the ratio 1:4, which applies for bulk heavy-hole excitons [52] and we treat the maximum intensity $A(\infty)$ as a fitting parameter. Results shown in figure 4(c) confirm the proportionality of the X^+ intensity to the population of holes with the relevant spin.

Note that we used the Maxwell–Boltzmann distribution to describe the population ratio at low hole density where the holes are likely to be localized [5, 13, 19]. The same assumption was done in [4] for a CdTe quantum well. At higher densities the full Fermi–Dirac distribution should be used. In spite of the fact that carriers of higher k-vectors give a smaller contribution to the absorption oscillator stength (as will be discussed later) it seems that even for relatively high hole gas concentrations the variation of the X^+ oscillator strength in magnetic field might be described as proportional to the hole population in one spin subband [23, 35].

An interesting case is the measurements in magnetic field of nonmagnetic quantum wells. For that system the Zeeman splitting is smaller than the Landau splitting and thus the complete spin polarization of electrons is observed only for magnetic field stronger than that at unit filling factor. For smaller fields the spin polarization is small and vanishes for each even filling factor. It was shown that the polarization of charged exciton absorption follows the polarization of carrier gas [63].

2.3. Line intensity in emission

In PL spectra the method of excitation and mechanisms of energy relaxation govern the relative intensity of X and X^+/X^- lines. Due to energy relaxation the PL spectra are dominated by the trion line for much lower carrier concentrations than in absorption. Increasing concentration makes relaxation to the lowest state (trion) more efficient and neutral exciton disappears. In most cases the system is far from thermal equilibrium between charged and neutral excitons. Typical CW experiments with nonresonant excitation involve many relaxation channels with very complex structure and over ten different characteristic times (even neglecting magnetic field—see figure 5) [64]. The nonresonant excitation creates hot nonequilibrium excitons, which thermalize down to radiative exciton states. Simultaneously or thereafter transitions between bright and dark exciton states occur. Already during thermalization the exciton may trap a carrier and form a charged exciton. After thermalization, the formation of charged excitons takes place from different neutral exciton states. The energy relaxation and charged exciton formation are continuously accompanied by radiative recombination of both kinds of exciton. Therefore, it is very difficult to determine all parameters of the complete system based only on CW data. Most of the formation rates depend on the spin of initial states. In order to deal with these problems many simplified pictures have been proposed. Some processes were neglected or different times were assumed to have the same value (for example radiative decay times of X and X^-). One very basic method is to use the chemical law of mass action and treat neutral and charged exciton populations as being in a kind of thermal quasi-equilibrium. Such an approach could only be justified when the formation/dissociation time of the charged exciton is much faster than the PL decay time. Then the system may reach thermal quasi-equilibrium before the majority of excitons is radiatively emitted. This condition is usually difficult to fulfil in the case of II–VI materials for which the radiative decay time is known to be rather short. An exception is possible at high temperatures, high carrier concentration, strong excitation or when the dissociation energy is very small [64–67]. For low excitation, when the density of excitons is much smaller than the density of pre-existing carriers the thermal equilibrium is given by the Boltzmann distribution. Then, taking into account X, $X^{+/-}$ and electron densities of states, the law of mass action can be written in the form

$$\frac{n_e n_X}{n_T} = 2\frac{k_B T}{\pi\hbar^2}\frac{m_e m_X}{m_T}\exp\left(-\frac{E_{diss}}{k_B T}\right) \qquad \text{or} \qquad \frac{n_X}{n_T} = \frac{2k_B T}{E_F}\frac{m_X}{m_T}\exp\left(-\frac{E_{diss}}{k_B T}\right) \tag{2}$$

where n_e, n_X and n_T denote carrier, neutral exciton and trion densities and m_e, m_X and m_T their respective masses. E_F is the carrier's Fermi energy, E_{diss} the charged exciton dissociation energy, T the temperature and k_B the Boltzmann constant. The PL intensities (I_X, I_T) are obtained by taking into account rates of radiative decays of thermalized neutral and charged exciton populations:

$$\frac{I_X}{I_T} = \frac{\tau_T}{\tau_X}\frac{n_X}{n_T}. \tag{3}$$

The opposite case is the case of low temperature when the process of charged exciton dissociation might be neglected. This condition is satisfied at temperatures below 30 K in the case of negatively charged excitons in an 8 nm CdTe/CdMgTe quantum well with $E_{diss} = 2.1$ meV and $n_e > 10^{10}$ cm^{-2}. In the case of quasi-equilibrium we would get $n_X/n_T \approx 0$. In reality the neutral exciton may be observed in these conditions, demonstrating a nonequilibrium situation. Then the rate equation model must be used. In that case different relaxation processes may be separated by use of resonant excitation. This was done in time-resolved experiments and a complete dynamics scheme was reconstructed [11].

3. Dynamics

3.1. Charged exciton formation

A charged exciton complex can be formed by light in two ways: directly by resonant excitation, or indirectly by excitation of an electron–hole pair or a neutral exciton which binds thereafter to a pre-existing carrier. The dynamics of both processes are different. In the first case (direct creation by light) the excitation pulse is followed by a monoexponential decay related to the radiative decay of charged excitons [22, 28]. This monoexponential temporal profile is perturbed if the temperature of the system is sufficiently high to cause thermal dissociation. The temperature limit depends on the dissociation energy of the charged exciton and on the carrier concentration. In the case of the CdTe-based QW discussed, the temperature limit related to a dissociation energy of about 2 meV is close to 30 K. An example of the temporal profile obtained for resonant excitation of the negatively charged exciton line in a $CdTe/Cd_{0.75}Mg_{0.25}Te$ quantum well is presented as a dashed curve in figure 6(a). In the case of nonresonant excitation the charged exciton luminescence exhibits both rise and decay times which strongly depend on the pre-existing carrier concentration. Typical temporal profiles of the signal detected on neutral and negatively charged excitons after excitation at neutral exciton energy are represented by solid curves in figures 6(a) and (b), at two different electron gas densities. In both cases the neutral exciton PL exhibits a fast experimentally unresolved rise time due to the resonant creation of cold excitons [5, 22, 44] and a biexponential decay. The fast initial decay is related to the transfer of the population of the neutral exciton bright states towards its dark states [44]. These dark states are either the $J = 1$ states with too large wavevectors to recombine radiatively, or the dipole-forbidden $J = 2$ states. The second, longer decay time constant represents the decay of the neutral exciton population after reaching a thermalized distribution between radiative and nonradiative states [32]. The negatively charged exciton (X^-) signal exhibits significant rise and decay time. However, the decay is different depending on the electron density. For low densities it is the same as that of thermalized neutral exciton PL, while for higher densities it is significantly slower and becomes equal to the value measured for direct excitation at X^- energy (75 ps). In order to describe both kinds of dynamic profile a simplified rate equation model presented schematically in figure 6(c) is used. All the excitonic states are approximated by only four levels (including the ground state of the crystal after recombination): the neutral exciton X continuum is divided into two levels representing the radiative and nonradiative states, and the charged exciton X^- is only represented by one level [33]. In the case of resonant excitation at X energy, four characteristic times are involved: $\tau_{X\,th}$—thermalization time of X population, $\tau_{X\,rad}$—radiative decay time of X, $\tau_{T\,form}$—formation time of X^-—and $\tau_{T\,rad}$—radiative lifetime of X^-. We assume here that the temperature is low enough to avoid dissociation of the charged excitons. After the first phase of X thermalization, the population of the X states is governed by only two times describing the probability of X recombination and X^- formation averaged over the X population. A further simplification is possible in the case of low electron concentration when the total neutral exciton decay rate $1/\tau_{X\,rad} + 1/\tau_{T\,form}$ is slower than the trion radiative rate $1/\tau_{T\,rad}$. Then the trions recombine fast after having been formed from neutral excitons and the PL of both lines decays asymptotically with the same rate: $1/\tau_{PL} = 1/\tau_{X\,rad} + 1/\tau_{T\,form}$ (see figure 1(a)). The ratio of the X and X^- populations is then given by equation (4):

$$\frac{n_X}{n_T} = \tau_{T\,form}\left(\frac{1}{\tau_{T\,rad}} - \frac{1}{\tau_{PL}}\right) \tag{4}$$

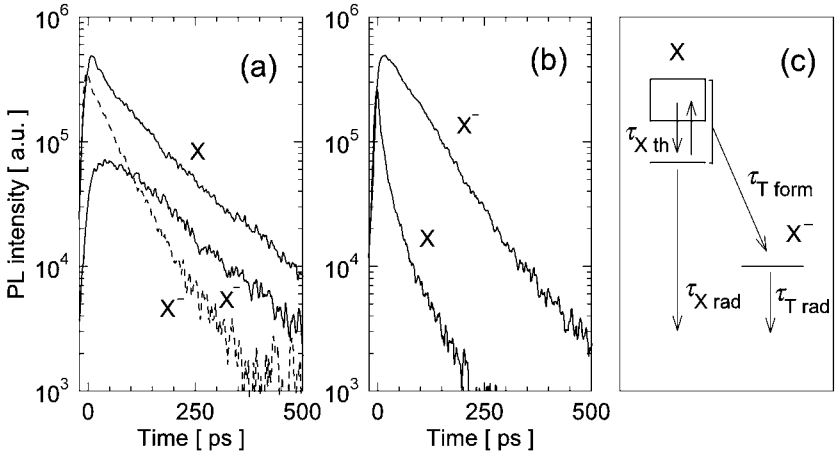

Figure 6. Temporal profiles of PL ((a) and (b)) for excitation in resonance at X^- (dashed curve) or X (solid curve) transition energy. The electron concentration in an 8 nm CdTe/$Cd_yMg_{1-y}Te$ quantum well was $\sim 1 \times 10^{10}$ cm^{-2} (a) and 5×10^{10} cm^{-2} (b); the temperature was 2 K. (c) Simplified scheme of levels and characteristic times [33] (graph from proceedings of *ICPS 2002* [68]).

from which the ratio of the X and X^- intensities may be expressed as

$$\frac{I_X}{I_T} = \left(\frac{\tau_{T\,form}}{\tau_{PL}} - 1\right)\left(1 - \frac{\tau_{T\,rad}}{\tau_{PL}}\right) \tag{5}$$

where I_X/I_T, τ_{PL} and $\tau_{T\,rad}$ can be determined directly from experiment (the last one by exciting resonantly charged excitons—dashed curve in figure 6(a)). Using this equation one can get the X^- formation time without doing the complex analysis of the whole PL temporal profiles. Thus, for the lowest concentration of about 10^{10} cm^{-2} the X^- formation time was found to be 500 ps. The formation time is observed to decrease with increasing electron concentration. Solving the rate equations allows one to show that when the neutral exciton decay rate $1/\tau_{X\,rad} + 1/\tau_{T\,form}$ becomes larger than the trion recombination rate $1/\tau_{T\,rad}$, the trion population, after having been fed by the decaying neutral excitons, decays asymptotically with its own characteristic time $\tau_{T\,rad}$. If in addition the formation of the trion is fast enough, it dominates the observed decay time of the neutral exciton. In the highest concentration range (5×10^{10} cm^{-2}) this time is reduced to less than 40 ps (figure 6(b)). The same variation of the formation time is observed for positively charged excitons. An example graph of the X^+ decay time (excitation at X energy) versus hole gas concentration is presented in figure 7(a). Below concentration $p = 3 \times 10^{10}$ cm^{-2} the decay time is governed by the X^+ formation rate. Above this concentration, the decay time becomes constant and close to the radiative decay obtained from measurements with resonant excitation at X^+ energy. For low carrier concentrations, the asymptotic ratio of X^+ and X intensities is used to obtain the formation time (equation (5)). Figure 7(b) shows that the formation time is inversely proportional to the pre-existing carrier concentration. Moreover, the values of the formation times for X^+ and X^- are comparable for similar concentrations [68]. This may be seen as a result of a dominant role of the neutral exciton mobility, for which the sign of pre-existing carriers is of minor importance (on top of the direct role of the charge concentration).

The role of the X mobility is additionally illustrated by the influence of X localization on the X^- formation time. The study was performed on a quantum well with disorder intentionally increased by alloy fluctuations in a QW made of alloy ($Cd_{1-x}Mn_xTe$). The excitation at

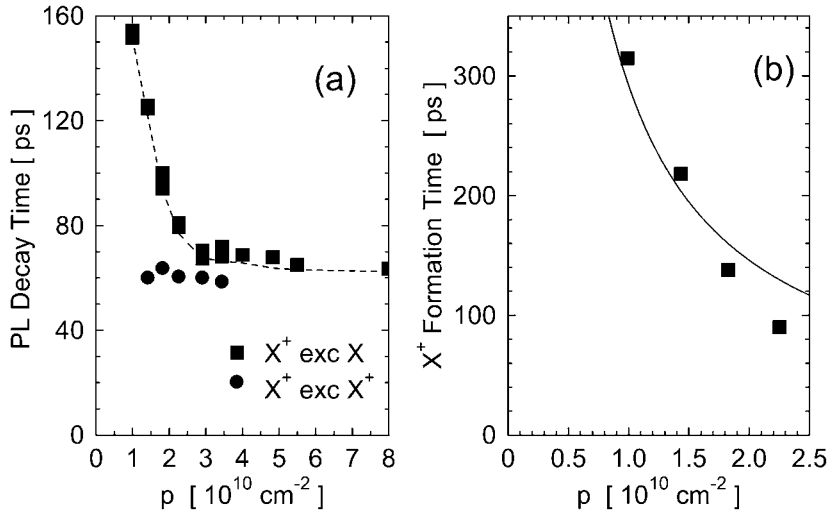

Figure 7. (a) PL decay time for excitation in resonance with X^+ (circles) or X (squares) and formation time of X^+ (b) versus hole gas concentration. The solid curve is proportional to the inverse of carrier density. Data obtained for an 8 nm wide $Cd_{0.998}Mn_{0.002}Te$ quantum well with $Cd_{0.66}Mg_{0.27}Zn_{0.07}Te$ barriers (graph from proceedings of *ICPS 2002* [68]).

different detunings from the X resonance allowed selection of exciton states either localized (excitation below the X maximum) or delocalized (at higher energy). The X^- formation time was found to be significantly longer for excitation at low energy [33]. It was interpreted as a signature that delocalized, mobile, neutral excitons form charged excitons faster than the localized ones (from the low-energy tail). This might be very important for the interpretation of relative intensities of X^- and X PL lines obtained in CW experiments. In particular their ratio cannot be simply used for the estimation of carrier gas concentration, without taking into account more complex properties of X states.

3.2. Recombination

The optical transitions related to creation or annihilation of neutral excitons were extensively studied by many authors (see for example [24]). The main qualitative difference between neutral and charged exciton transitions is related to a different initial state (in absorption) or final state (in emission). For a neutral exciton this state is the state with no band carriers. Therefore the conservation of momentum and small wavevector of light allows a very small range of exciton k-vectors to be optically active. In contrast, the final state of charged exciton recombination consists of a one-carrier state. Thus the charged exciton with k-vectors larger than zero can also recombine radiatively as its momentum can be transferred to the remaining particle. Therefore, a larger population of charged excitons with higher k-vectors is involved in the optical transitions. However, the probability of transition depends on the overlap between the wavefunction of the final free carrier and that of the charged exciton. It decreases with increasing momentum of both particles. The probability of optical transitions was calculated first by Stébé *et al* for absorption [25] and later by Esser *et al* [21] for luminescence. It was shown [21] that the matrix element between initial and final states can be approximated by an exponential function: $|M(k)|^2 \sim \exp(-\varepsilon(k)/\varepsilon_1)$, where $\varepsilon(k) = \hbar^2 k^2 M_X/2mM_T$, and where k denotes the total momentum of the trion or carrier; M_X, m and $M_T = M_X + m$ are the mass of

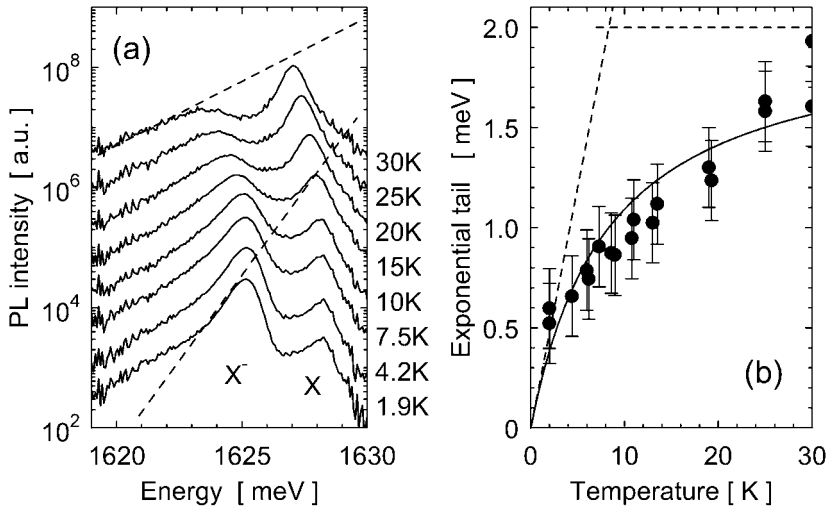

Figure 8. CW-PL spectra (a) of an n-doped 8 nm CdTe/$Cd_yMg_{1-y}Te$ quantum well at indicated temperatures. The dashed lines represent the expected slopes of low-energy tails at two selected temperatures. (b) Fitted values of the decay constant E_{tail} of the X^- exponential spectral tail as a function of temperature (graph from proceedings of *ICPS 2002* [68]).

the neutral exciton, electron and trion. The characteristic energy ε_1 was obtained numerically and was equal, for example, to 2 or 0.6 meV for X^- or X^+ states respectively in an 8 nm wide CdTe quantum well with $Cd_{0.7}Mg_{0.3}Te$ barriers. This expression of the matrix element explains well the results of several optical experiments.

First of all, the PL intensity can be described by using the Fermi golden rule and a thermal distribution of trion states. The Boltzmann distribution of trions can be applied for experiments, done with a reasonably small excitation density. Neglecting broadening mechanisms, the calculated shape of the PL line is asymmetric and has an exponential tail on the low-energy side (note that larger wavevectors correspond to lower transition energies due to the mass difference between the trion and the carrier). The characteristic energy E_{tail} of this tail is given by $1/E_{tail} = (1/k_BT)(m/M_X) + 1/\varepsilon_1$. The first term due to the Boltzmann distribution dominates at low temperatures and leads to an initially linear increase of E_{tail} with temperature. At higher temperatures, as higher k-states of X_T are increasingly populated, the optical matrix element sets the maximum characteristic energy of the spectral tail at ε_1. Experimentally, such a behaviour was observed in PL measured as a function of temperature [21, 22]. Typical spectra obtained for the X^- line in a CdTe/$Cd_{0.75}Mg_{0.25}Te$ quantum well are presented in figure 8(a). The dashed lines show the predicted slopes of the tail at the highest and lowest temperatures for which either of the two individual components is dominant. Figure 8(b) demonstrates a good agreement of the temperature variation of the PL tail characteristic energy with the model. However, one should note here that a correct description of the whole PL line-shape must involve homogeneous and inhomogeneous broadening. The X^- line of figure 8(a) also shows a second tail at lower energy with a smaller temperature-independent slope. This tail is due to localized trion states [33]. Such states cannot be correctly described by a simple trion model, but it was found that describing localization through an effective spread of trion states over k-space one obtains a correct prediction of the low-energy tail.

The PL radiative decay time is inversely proportional to the average of the emission probabilities of all populated k-states. Radiative decay time increases linearly with temperature

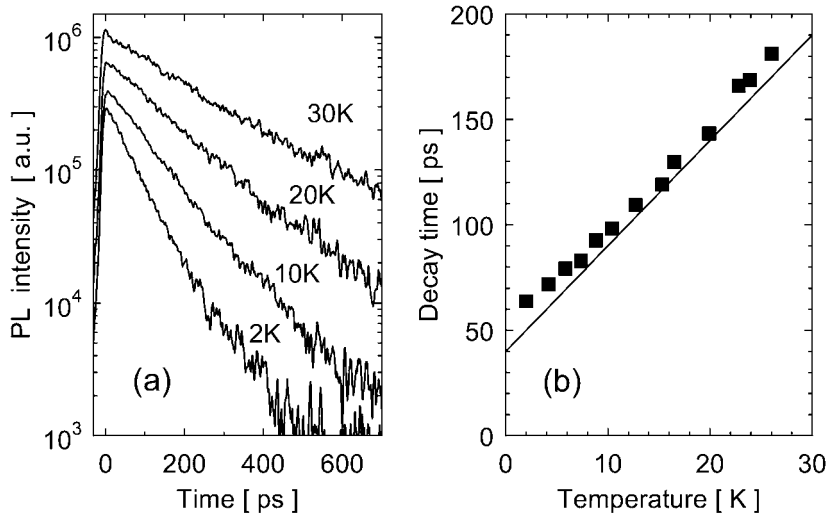

Figure 9. Time-resolved X^- PL spectra for different temperatures (a) and decay time of the X^- PL as a function of temperature (b). The lines give the predictions of the model [22]. Data obtained for an n-doped 8 nm CdTe/Cd_yMg_{1-y}Te quantum well (graph from proceedings of *ICPS 2002* [68]).

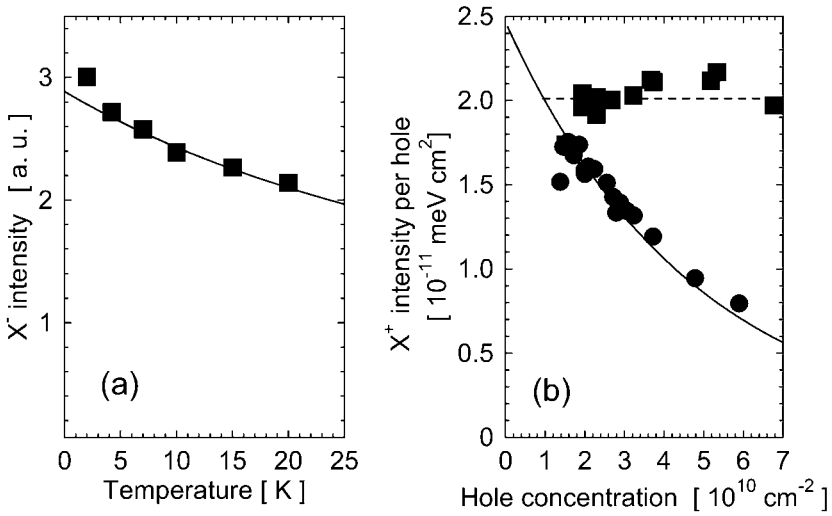

Figure 10. (a) Integrated intensity of X^- extracted from reflectivity (points) and comparison with the rescaled inverse trion lifetime (solid curve). (b) Integrated intensity of X^+ transmission line per hole versus hole concentration (circles) compared to the oscillator strength extracted from inverse trion lifetime (squares) [27] (graph from proceedings of *ICPS* [68]).

as the maximum recombination probability is close to $k = 0$ and the population of these states decreases with temperature. An experimental check was made by time-resolved measurements of PL [22]. Temporal profiles of negative trion PL intensity after pulse resonant excitation are shown in figure 9(a). The calculated radiative lifetimes of X^- were in good agreement with the measurements (figure 9(b)). Only below 7 K did the X^- lifetime deviate from the linear dependence, tending towards a constant value. This behaviour is typical of the influence of localization on the lifetime.

3.3. Decay rate versus absorption line intensity

The probability of emission is directly related to the oscillator strength in absorption. The Boltzmann thermal distribution of X^- is replaced by the thermal distribution of the electron, which is now the initial state. If the concentration of carriers is increased then the Boltzmann distribution of carriers has to be replaced by the Fermi–Dirac distribution. As a result, even at low temperature, the increasing carrier concentration results in populating states with higher k-vector. Therefore, the probability of optical transition per carrier is reduced. Such an experiment was done in transmission for positively charged excitons in a modulation-doped $Cd_{0.998}Mn_{0.02}Te$ quantum well [27]. The oscillator strength per hole $A(p)/p$ is presented in figure 10(b) (circles). The solid curve in figure 10(b) was obtained numerically assuming Fermi–Dirac distribution of the pre-existing holes in the quantum well at $T = 2$ K. It shows an excellent agreement with the experimental data. It is interesting to point out that the oscillator strength per carrier obtained from transmission measurement can be compared to the radiative PL lifetime. The quantitative comparison of both kinds of datum (PL and absorption) can be done using an atomic-like formula [24, 30], which has been successfully applied for excitons bound to impurities:

$$\frac{\hbar}{\tau} = \frac{n^2\omega^2}{3\pi^2c^2}A(p)/p \tag{6}$$

where n is the refractive index, c the velocity of light and ω the frequency. The expected oscillator strength $A(p)/p$ extracted from PL lifetime measurements [27] and taking into account the effect of the cap layer [23, 31] is shown by squares in figure 10(b). One notices a good agreement between both experiments for the smallest hole density, while for the higher ones the difference increases and reaches a factor of two for $p = 4\times10^{10}\,\mathrm{cm}^{-2}$. This difference is relatively obvious since in the PL experiment, as opposed to the absorption, only few initial states are populated. Therefore, the charged exciton may thermalize to states of k-vector close to zero for any hole concentration.

For low electron concentrations, the electron gas is nondegenerate and its thermal distribution also follows a Boltzmann distribution. The main difference between absorption and emission at low electron densities is due to the difference in masses between X^- or X^+ and free carrier. Therefore, one can compare directly the temperature variation of the lifetime, and the absorption when the temperature axis is rescaled by m/M_T. The result obtained from reflectivity measurements [22] on a negatively charged exciton transition (figure 10(a)) demonstrates a good agreement between the measured variations of the radiative lifetime and the absorption of X^-. This can be seen as another argument of the applicability of the simple three-particle model of the free trion.

Summarizing, a decrease of trion oscillator strength is always observed when initial states of higher k-vector are populated. It might be caused by an increase of temperature or by the Pauli exclusion rule when increasing the carrier concentration. The same effect is observed in absorption and in emission experiments. This is in contrast to the behaviour of the neutral exciton for which the radiative decay time increases with temperature but absorption oscillator strength remains almost constant.

3.4. Spin of the charged exciton

So far we have discussed dynamics of charged excitons neglecting phenomena related to spin relaxation. The trion state consists of two majority and one minority carriers. Both types of carrier may have two orientations of angular momentum (in a usual quantum well $\pm3/2$ for a heavy hole and $\pm1/2$ for a electron). In zero magnetic field the singlet state is a fundamental

state. In the singlet state the total angular momentum is equal to the momentum of the minority carrier (hole in X^- and electron in X^+). The triplet state is observed only in high magnetic field or when Zeeman splitting is larger than singlet–triplet splitting [17, 56].

The singlet state of the trion due to its simplicity is particularly suitable for a spin flip study. It is well known that spin relaxation is very important for understanding dynamics related to neutral exciton. But the whole system is complex and involves at least four spin states (two dark and two bright) [69]. In normal optical experiments, only bright states can be observed. But the relaxation from one bright state (excited by circularly polarized light) to the other one involves transitions between all exciton spin states. Therefore different characteristic times are involved for different spin flip processes. The complete description of spin dynamics is only possible after a detailed and complex fitting procedure [69, 70]. The spin flip process is much simpler for the (singlet) charged exciton. It involves only two spin states of the trion and is governed by the flip of an electron (for X^+) or a hole (for X^-). Moreover the absence of dark states makes polarization analysis much easier than in the case of the neutral exciton [11].

The simplest experimental approach is based on resonant excitation of charged exciton states. The transition is excited by a pulse of circularly polarized light and the PL is analysed in both circular polarizations. Then, there are two possibilities: either degree of circular polarization is analysed or spin relaxation is measured directly as the rise time of the PL excited by circularly polarized light of opposite helicity.

We will first discuss the second possibility which was exploited for n-type quantum wells [45, 46]. The PL was excited by a mode-locked titanium sapphire laser. The signal was collected by a streak camera with resolution better than 4 ps. Any significant heating of the carrier gas was avoided by the use of very low excitations ($<$50 pJ cm^{-2}). The excitation with energy lower than that of the neutral exciton transition assured a precise selection of the states participating in spin relaxation. In particular, no neutral exciton states were created. Therefore, the whole spin relaxation process was determined by the spin flip of the hole in the singlet state of the charged exciton. The typical temporal profiles of the PL signal from a CdTe/$Cd_{0.75}Mg_{0.25}$Te quantum well are presented in figure 11(a) for two different excitation energies. The data are well described by the simple two-level rate equation model with two parameters (rise time τ_R and decay time τ_{dec}). The decay time was found to be always about 65 ps, in good agreement with the values discussed in section 3.2 for radiative recombination of X^- in CdTe-based quantum wells [22]. The spin relaxation time τ_{SF} was obtained from the rise and decay times using the relation $1/\tau_{SF} = 1/\tau_R - 1/\tau_{dec}$. The measurements were performed for different excitation energies. Example results of the excitation energy scan are presented in figure 11(b). At 4×10^{10} holes cm^{-2} it was found that the relaxation time is about 35 ps, when the excitation coincides with the energy of the PL peak. When varying the excitation energy from the PL peak to the absorption maximum, a decrease of the relaxation time from 35 to 8 ps was observed. This means that charged excitons possessing a higher kinetic energy exhibit faster spin relaxation. One should note, however, that the lower limit of relaxation time must be taken with caution. The lowest measured value is limited by the energy relaxation within the spin subband. This time was estimated experimentally by the measurement of the PL rise time with crossed linear polarizations of excitation and detection. Indeed, we found that the rise time is increasing with increasing excitation energy and approaches the value measured in crossed circular polarizations ($\sim$5 ps). This shows the natural limit of the experiment; however, longer relaxation times are reliable and can be interpreted as a spin flip time of the heavy hole forming the singlet trion state.

The higher limit 35 ps represents a spin relaxation of the hole in the cold charged exciton in the state which dominates in the radiative transition. The excitation in higher energy leads to the formation of states possessing a nonzero kinetic energy and most of the radiative recombination

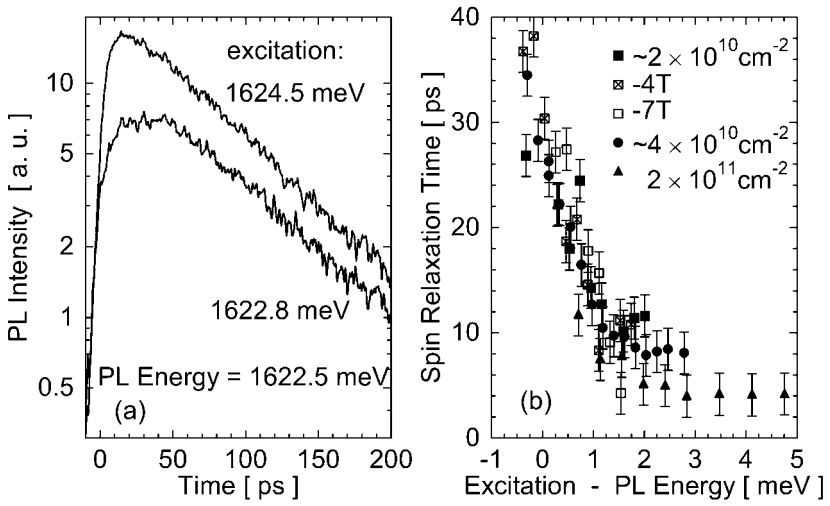

Figure 11. Time-resolved X^- PL spectra detected in cross-circular polarization with respect to excitation for two different excitation energies (a). Spin relaxation time as a function of the energy difference between the excitation energy and the X^- PL maximum for three different electron concentrations (full symbols) and for $n_e = 2 \times 10^{10}$ cm^{-2} at different magnetic fields (open symbols) (b). Data for n-type 8 nm CdTe/Cd_yMg_{1-y}Te quantum well (data from [46]).

takes place after the energy relaxation. The spin flip time versus excess energy presented in figure 11(b) was measured for three different concentrations of electron gas. It is interesting to note that the observed times hardly depend on the concentration over the whole range used in experiment (from 2×10^{10} to about 2×10^{11} cm^{-2}). The experimentally observed variation of the spin flip time with increasing excitation energy has been predicted and observed for free holes in QWs [47, 48]. Indeed, for $k > 0$, the heavy and light hole states are mixed and the hole spin state is no longer pure. Any energy or momentum relaxation process can then lead to spin relaxation. Such an explanation can be applied to X^-. However, a quantitative comparison with the existing theories or measurements of free hole spin flip is not straightforward. Free holes have been predicted to have an infinite relaxation time at $k = 0$ [47]. Such long spin flip times cannot be observed for holes bound in excitonic complexes whose radiative bound states are also constituted of hole states which are far from $k = 0$. A decrease of the spin flip time might be interpreted in terms of well known mechanisms of spin relaxation such as Bir–Aronov–Pikus and Dyakonov–Perel. Both of them lead to a reduction of the hot carrier spin flip time in comparison to the cold one (see also [11, 48, 49]). However, the weak influence of the electron concentration suggests negligible importance of relaxation processes based on the scattering on free carriers. It allows exclusion of some of the spin relaxation channels.

To try to distinguish between different spin flip mechanisms, the spin flip time was studied not only as a function of electron concentration but also as a function of magnetic field. The studied QW has been engineered so that by applying a magnetic field, one can change the occupation factor of the initial electron states without influencing the spin splitting of the X^- singlet state. For the used sample the hole g-factor is zero while the electron g-factor equals -1.46 [8, 50]. Thus, as the X^- Zeeman splitting of the X^- singlet state is solely determined by the hole g-factor, the electron gas can be polarized without affecting the spin splitting of the X^- singlet state. At high magnetic field ($\sim$5 T) the only available electrons have a spin of $+1/2$. This should strongly suppress the spin flip of the $+3/2$ hole in X^-

when considering the exchange interaction mechanism. The respective spin flip times are presented as open symbols in figure 11(b) and are observed to be relatively insensitive to the experimental conditions. However, the varied parameters influence the number of available electrons on which the hole can scatter and flip its spin via the exchange interaction. This is the so called Bir–Aronov–Pikus mechanism which involves the simultaneous spin flip of a hole and an electron. Its efficiency is proportional to to the occupation factor of the initial electron states and to the number of available final states.

As no significant slowdown of the X^- spin relaxation was observed under magnetic field, it was concluded that the Bir–Aronov–Pikus spin flip mechanism is not the most important one for the negative trions. This may well be a general feature of the hole spin flip in X^-. Indeed, the strength of the exchange interaction depends strongly on the relative distance between the electron and hole. As X^- is negatively charged, it repels the surrounding electrons; this weakens the effect of the exchange interaction. Further investigations are needed to make this a general statement as well as to determine what is the mechanism responsible for the X^- spin flip. It is to be noted that the experiment in magnetic field might be complicated by the X^- spin triplet line. It can appear around the X energy [17, 56] and may possibly complicate the spin relaxation. However, this line has not been observed either in PL or reflectivity in the above-discussed work and therefore its influence was not considered.

Another experimental possibility to study the charged exciton spin relaxation is to analyse the degree of circular polarization after excitation by a circularly polarized light pulse. In principle both methods should give the same result but in real experiments they are sensitive to slightly different ranges of the complex relaxation process. The direct measurement of the PL rise time probes the fast initial relaxation mechanisms, which are usually combined with the energy relaxation. The longer times are often masked by decay of PL and are difficult or impossible to resolve. The polarization degree is also sensitive for longer times when a very small difference between intensities in both circular polarizations is observed. An example comparison of both kinds of datum obtained for the same sample and in the same experimental conditions is presented in figures 12(a) and (b). The dynamics of the PL and polarization degree were obtained for the same conditions as those of figure 11(a).

It is seen that polarization degree $P = (I_{\sigma+} - I_{\sigma-})/(I_{\sigma+} + I_{\sigma-})$ decays with a time constant of about 30 ps which corresponds to the spin relaxation for trion states excited resonantly in the energy of the trion PL line. This time constant of polarization decay does not vary noticeably with excitation energy, even if excitation energy is tuned almost to the X energy [71]. This shows that independently of excitation energy (within this range) the charged excitons relax to the same lowest states for which relaxation time was about 30 ps. The only trace of the first relaxation is the initial polarization which is significantly lower than unity. The analysis of polarization degree is more sensitive for longer times. This technique was extensively used in studies of charged exciton spin relaxation for positively and negatively charged excitons by [11, 49].

3.5. Charged exciton localization

In a great part of the discussion presented so far, it has been assumed that charged excitons are delocalized three-particle complexes. The most obvious limit of such an approach is a localization in any kind of disorder, e.g., resulting from Coulomb potential of ionized donors or acceptors [73]. The presence of such centres is a natural consequence of the doping used to introduce carrier gas to the quantum well. The depth and size of potential fluctuations depends on the distance between doping and quantum well as well as on the doping density. If doping is close to the quantum well the exciton complex should be considered as D^0X or

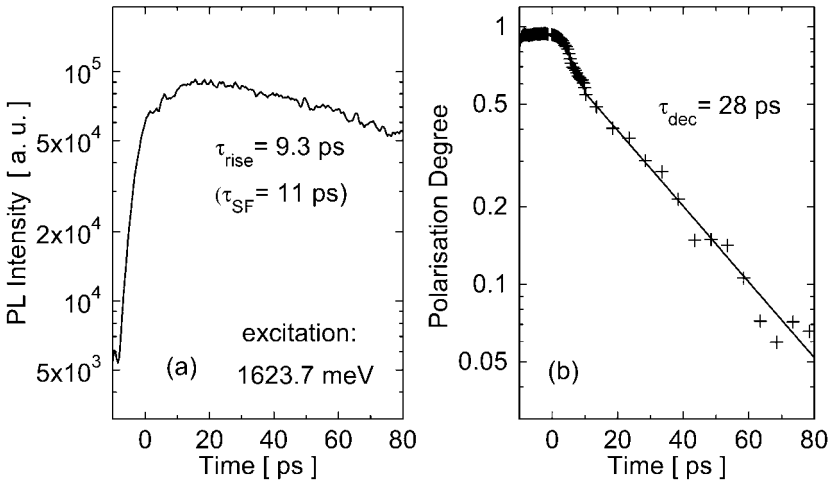

Figure 12. Comparison of a time-resolved X^- PL spectrum detected in cross-circular polarization (a) with temporal evolution of PL polarization degree (b) obtained in the same conditions for an 8 nm CdTe/Cd_yMg_{1-y}Te quantum well with $n_e = 2 \times 10^{10}$ cm^{-2} (data from [46]).

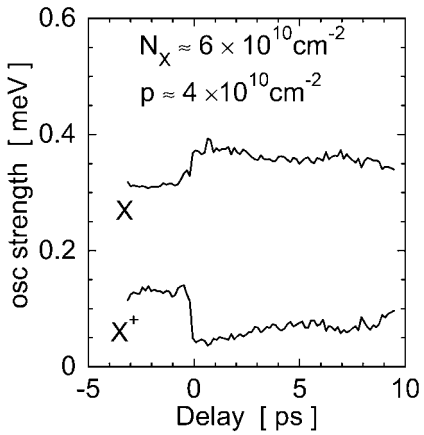

Figure 13. X and X^+ oscillator strength extracted from transmission spectra in pump–probe experiment as a function of delay between pulses [34]. Data for a p-type 8 nm $Cd_{0.998}Mn_{0.002}$Te/ $Cd_{0.66}Mg_{0.27}Zn_{0.07}$Te quantum well (graph from proceedings of *ICPS* [68]).

A ^{0}X [4, 30, 72]. For weak localization the difference between D ^{0}X or A ^{0}X and the localized trion is a matter of terminology and differentiating should be based on analysed properties. Independently of the nature of the localizing potential, there are two limits of the localization. If the localization length is small, the wavefunction of the charged exciton is significantly perturbed. In that case, the model of the free trion discussed before (section 3.2) cannot be applied. It is necessary to perform three-particle calculations with defined confining potential. If the confining potential is a Coulomb one, the problem rather resembles the problem of D ^{0}X or A ^{0}X complexes. The other limit is the localization in shallow, long-range fluctuations of potential. Then the localization range is long in comparison to the charged exciton size and the charged exciton might be treated as a quasiparticle of a given centre of mass motion. The wavefunction of such a localized state is composed of trion three-particle wavefunctions of

different k-vectors. As localization length is smaller the higher k-vectors are more important. In order to describe an optical transition, it is possible to employ an approach similar to that used for thermal distribution of free trion states. Therefore, charged exciton localization results in an asymmetry of the PL line with a low-energy tail even at the lowest temperatures [68]. PL spectra showing such tails were observed for several samples containing negatively charged excitons. Example spectra are presented in figure 8(a). The length of the low-energy tails is limited by the value of the ε_1 parameter, in the same way as it was limited for the temperature dependence of the PL line shape of free trion origin. This explains why the tails due to localized states do not change too much with temperature in figure 8(a).

The increasing contribution of higher k-vector components leads to a decrease of optical transition probability and an increase of PL decay time. This explains the deviation from the linear dependence of X^- lifetime on temperature, observed below 7 K by Ciulin *et al* [22] (figure 9(b)). On the other hand, the agreement of the measured decay times with the predictions of the free trion model shows that for higher temperatures the charged excitons might be treated as free. This means that the localization length is longer than the length corresponding to k-vectors of thermally excited charged excitons.

A more difficult experimental proof for delocalization of charged excitons would be observation of diffusion or transport under applied tension [74, 75]. There have been attempts to find such phenomena in II–VI quantum wells by time-resolved micro-PL and degenerate four-wave mixing [15, 19, 58]. They show that above a certain temperature diffusion of the charged exciton is observed.

4. Beyond the simple trion model

In the preceding paragraph we discussed some possibilities to generalize the three-particle model of the free charged exciton to account for localization effects. However, there are phenomena escaping this model. The linear variation of the charged exciton dissociation energy with carrier concentration, discussed in section 2.1, is a clear demonstration of the influence of the whole population of carriers present in the quantum well, and therefore cannot be described in a three-particle trion model.

A second example of phenomena requiring a departure from the simple model is the relation between oscillator strengths of neutral and charged excitons. It was pointed out by Kheng in [4] that the appearance of charged exciton absorption is accompanied by a decrease of the oscillator strength of the neutral exciton. This phenomenon, named oscillator strength stealing, is observed when changing the concentration of pre-existing unpolarized carriers [23, 55], as well as polarizing a constant density of pre-existing carriers [23]. It was also confirmed by an observation of quantum beats [19] and measurements of Rabi splitting in doped quantum wells embedded in a microcavity [20]. Such a phenomenon is similar to the optical sum rule but, in contrast to the cases of the exciton and biexciton [42], the sum of oscillator strengths is not conserved. This shows that neutral and charged excitons cannot be considered as states isolated from other states belonging to the continuum.

Furthermore, the enhancement of the oscillator strength of the neutral exciton is observed not only when the charged exciton is quenched by removing the pre-existing carriers of proper spin, but also through the saturation of the pre-existing carriers by a strong laser pulse [34]. Figure 13 shows the variation of the X and X^+ absorption intensities in a pump and probe experiment, after a strong femtosecond pump pulse. The pump pulse created concentration of excitons comparable to the concentration of pre-existing carriers. Therefore, the X^+ absorption was quenched as almost all holes formed charged complexes, and this was accompanied by an increase of the absorption due to the neutral exciton [76].

5. Conclusions

A review of the optical studies of doped II–VI quantum wells demonstrates a wealth of properties of exciton states, neutral as well as positively and negatively charged. A wide range of optical measurements and of experimental conditions yielded the values of various fundamental parameters of the excitonic states. These include their energies, optical transition probabilities and characteristic times of their formation, thermalization and decay. A model of a free three-particle charged exciton developed by Stébé *et al* [25] and Esser *et al* [21] was shown to describe correctly the results of many of the experiments. However, some of them require a departure from the simple model. In particular, the variation of the charged exciton dissociation energy or the excitonic oscillator strengths with carrier concentration show that the charged exciton represents in fact a collective excitation of the free carrier sea in the presence of a carrier of opposite sign.

Acknowledgments

I would like to thank my collaborators V Ciulin, J Cibert, A Esser, M Kutrowski, W Maślana, D Ferrand, P Płochocka S Tatarenko, T Wojtowicz, J Kossut and B Deveaud. I am particularly thankful to J A Gaj for help and stimulating discussions. This work is partially supported by the Polish–French Collaboration Program Polonium and Polish Committee for Science (KBN) grant 5 P03B 023 20.

References

[1] Lampert M A 1958 *Phys. Rev. Lett.* **1** 450
[2] Thomas G A and Rice T M 1977 *Solid State Commun.* **23** 359
[3] Kawabata T, Muro K and Narita S 1977 *Solid State Commun.* **23** 267
[4] Kheng K, Cox R T, Merle d'Aubigné Y, Franck Bassani, Saminadayar K and Tatarenko S 1993 *Phys. Rev. Lett.* **71** 1752
[5] Finkelstein G, Shtrikman H and Bar-Joseph I 1995 *Phys. Rev. Lett.* **74** 976
[6] Shields A J, Osborne J L, Simmons M Y, Pepper M and Ritchie D A 1995 *Phys. Rev.* B **52** R5523
[7] Haury A, Arnoult A, Chitta V A, Cibert J, Merle d'Aubigné Y, Tatarenko S and Wasiela A 1998 *Superlatt. Microstruct.* **23** 1097
[8] Wojtowicz T, Kutrowski M, Karczewski G, Kossut J, Teran F J and Potemski M 1999 *Phys. Rev.* B **59** R10437
Wojtowicz T, Kutrowski M, Karczewski G and Kossut J 1998 *Appl. Phys. Lett.* **73** 1379
[9] Astakhov G V, Yakovlev D R, Kochereshko V P, Ossau W, Nürnberger J, Faschinger W and Landwehr G 1999 *Phys. Rev.* B **60** R8485
[10] Lovisa S, Cox R T, Magnea N and Saminadayar K 1997 *Phys. Rev.* B **56** R12787
[11] Vanelle E, Paillard M, Marie X, Amand T, Gilliot P, Brinkmann D, Lévy R, Cibert J and Tatarenko S 2000 *Phys. Rev.* B **62** 2696
[12] Kheng K, Cox R T, Baron T, Saminadayar K and Tatarenko S 1996 *J. Cryst. Growth* **159** 443
[13] Eytan G, Yayon Y, Rappaport M, Shtrikman H and Bar-Joseph I 1998 *Phys. Rev. Lett.* **81** 1666
[14] Brinkmann D, Kudrna J, Gilliot P, Hönerlage B, Arnoult A, Cibert J and Tatarenko S 1999 *Phys. Rev.* B **60** 4474
[15] Wagner H P, Tranitz H-P and Schuster R 1999 *Phys. Rev.* B **60** 15542
[16] Yoon H W, Ron A, Sturge M D and Pfeiffer L N 1996 *Solid State Commun.* **100** 743
[17] Shields A J, Pepper M, Simmons M Y and Ritchie D A 1995 *Phys. Rev.* B **52** 7841
[18] Crooker S A, Johnston-Halperin E, Awschalom D D, Knobel R and Samarth N 2000 *Phys. Rev.* B **61** R16307
[19] Gilliot P, Brinkmann D, Kudrna J, Crégut O, Lévy R, Arnoult A, Cibert J and Tatarenko S 1999 *Phys. Rev.* B **60** 5797
[20] Brunhes T, André R, Arnoult A, Cibert J and Wasiela A 1999 *Phys. Rev.* B **60** 11568
[21] Esser A, Runge E, Zimmermann R and Langbein W 2000 *Phys. Rev.* B **62** 8232
[22] Ciulin V, Kossacki P, Haacke S, Ganière J-D, Deveaud B, Esser A, Kutrowski M and Wojtowicz T 2000 *Phys. Rev.* B **62** R16310

[23] Kossacki P, Cibert J, Ferrand D, Merle d'Aubigné Y, Arnoult A, Wasiela A, Tatarenko S and Gaj J A 1999 *Phys. Rev.* B **60** 16018
[24] Andreani L C 1994 *Confined Electrons and Photons, New Physics and Applications* ed E Burnstein and C Weisbuch (New York: Plenum)
[25] Stébé B, Feddi E, Ainane A and Dujardin F 1998 *Phys. Rev.* B **58** 9926 and references therein
[26] Volkov O V, Zhitomirskii V E, Kukushkin I V, Bisti V E, von Klitzing K and Eberl K 1997 *JETP Lett.* **66** 766
[27] Kossacki P, Ciulin V, Cibert J, Merle d'Aubigné Y, Arnoult A, Bourgognon C, Wasiela A, Tatarenko S, Staehli J-L, Ganière J-D, Deveaud B and Gaj J A 2000 *J. Cryst. Growth* **214/215** 837
[28] Finkelstein G, Umansky V, Bar-Joseph I, Ciulin V, Haacke S, Ganière J-D and Deveaud B 1998 *Phys. Rev.* B **58** 12637
[29] Mayer E J, Pelekanos N T, Kuhl J, Magnea N and Mariette H 1995 *Phys. Rev.* B **51** 17263
[30] Kheng K 1995 *Ann. Phys., Paris* **20** C2 229
[31] Merle d'Aubigné Y, Wasiela A, Mariette H and Dietl T 1996 *Phys. Rev.* B **54** 14003
[32] Vinattieri A, Shah J, Damen T C, Kim D S, Pfeiffer L N, Maiallc M Z and Sham L J 1994 *Phys. Rev.* B **50** 10868
[33] Kossacki P, Ciulin V, Kutrowski M, Ganière J-D, Wojtowicz T and Deveaud B 2002 *Phys. Status Solidi* b **229** 659
[34] Płochocka P, Kossacki P, Cibert J, Maślana W, Tatarenko S, Radzewicz C and Gaj J A 2002 *Acta Phys. Pol.* A **102** 679
[35] Maślana W, Bertolini M, Boukari H, Kossacki P, Ferrand D, Gaj J A, Tatarenko S and Cibert J 2003 *Appl. Phys. Lett.* at press
(Maślana W, Bertolini M, Boukari H, Kossacki P, Ferrand D, Gaj J A, Tatarenko S and Cibert J 2002 *Preprint* cond-mat/0207259)
[36] Kossacki P 2001 *Acta Phys. Pol.* A **100** 237
[37] Huard V, Cox R, Saminadayar K, Arnoult A and Tatarenko S 2000 *Phys. Rev. Lett.* **84** 187
[38] Cole B E, Takamasu T, Takehana K, Goldhahn R, Schulze D, Kido G, Chamberlain J M, Gobsch G, Henini M and Hill G 1998 *Physica* B **249–251** 607
[39] Astakhov G V, Yakovlev D R, Kochereshko V P, Ossau W, Faschinger W, Puls J, Hanneberger F, Crooker S A, McCulloch Q, Wolverson D, Gippius N A and Waag A 2002 *Phys. Rev.* B **65** 165335
[40] Hawrylak P 1991 *Phys. Rev.* B **44** 3821
Brown S A, Young J F, Brum J A, Hawrylak P and Wasilewski Z 1996 *Phys. Rev.* B **54** R11082
[41] Suris R A, Kochereshko V P, Astakhov G V, Yakovlev D R, Ossau W, Nurnberger J, Faschinger W, Landwehr G, Wojtowicz T, Karczewski G and Kossut J 2001 *Phys. Status Solidi* b **227** 343
[42] Saba M, Quochi F, Ciuti C, Oesterle U, Staehli J L, Deveaud B, Bongiovanni G and Mura A 2000 *Phys. Rev. Lett.* **85** 385
[43] Sanvitto D, Pulizzi F, Shields A J, Christianen P P C M, Holmes S N, Simmons M Y, Ritchie D A, Maan J C and Pepper M 2001 *Science* **294** 837
[44] Deveaud B, Clérot F, Roy N, Satzke K, Sermage B and Katzer D S 1991 *Phys. Rev. Lett.* **67** 2355
[45] Kossacki P *et al* 2000 *Proc. Int. Conf. on Physics of Semiconductors (Osaka, 2000)* (Berlin: Springer) p 623
[46] Ciulin V, Kossacki P, Kutrowski M, Ganiere J-D, Wojtowicz T and Deveaud B 2002 *Phys. Status Solidi* b **229** 627
[47] Fereira R and Bastard G 1991 *Phys. Rev.* B **43** 9687
[48] Baylac B *et al* 1995 *Solid State Commun.* **93** 57
[49] Vanelle E *et al* 2000 *Proc. Int. Conf. on Physics of Semiconductors (Osaka, 2000)* (Berlin: Springer)
[50] Sirenko A A *et al* 1997 *Phys. Rev.* B **56** 2114
[51] Gaj J A, Grieshaber W, Bodin-Deshayes C, Cibert J, Feuillet G, Merle d'Aubigné Y and Wasiela A 1994 *Phys. Rev.* B **50** 5512
[52] Gaj J A, Planel R and Fishman G 1979 *Solid State Commun.* **29** 435
[53] Lovisa S, Cox R T, Baron T, Keim M, Waag A and Landwehr G 1998 *Appl. Phys. Lett.* **73** 656
[54] Lovisa S, Cox R T, Magnea N and Saminadayar K 1998 *J. Cryst. Growth* **184/185** 810
[55] Miller R B, Baron T, Cox R T and Saminadayar K 1998 *J. Cryst. Growth* **184/185** 822
[56] Yusa G, Shtrikman H and Bar-Joseph I 2001 *Phys. Rev. Lett.* **87** 216402
[57] Yokoi H, Kakudate Y, Fujiwara S, Kim Y, Takeyama S, Karczewski G, Wojtowicz T and Kossut J 2002 *Phys. Status Solidi* b **229** 681
[58] Portella-Oberli M T, Ciulin V, Haacke S, Ganiere J-D, Kossacki P, Kutrowski M, Wojtowicz T and Deveaud B 2002 *Phys. Rev.* B **66** 155035
[59] Redliński P and Kossut J 2001 *Solid State Commun.* **118** 295
[60] Riva C, Peeters F M and Varga K 2000 *Phys. Rev.* B **61** 13873
[61] Stébé B, Munschy G, Stauffer L, Dujardin F and Murat J 1997 *Phys. Rev.* B **56** 12454

[62] Kutrowski M 2001 *PhD Thesis* Institute of Physics Polish Academy of Sciences
[63] Astakhov G V, Kochereshko V P, Yakovlev D R, Ossau W, Nurnberger J, Faschinger W, Landwehr G, Wojtowicz T, Karczewski G and Kossut J 2002 *Phys. Rev.* B **65** 115310
[64] Jeukens C R L P N, Christianen P C M, Maan J C, Yakovlev D R, Ossau W, Wojtowicz T, Karczewski G and Kossut J 2002 *Phys. Status Solidi* a **190** 813
[65] Manassen A, Cohen E, Arza R, Linder E and Pfeiffer L N 1996 *Phys. Rev.* B **54** 10609
[66] Arza R, Yoon H W, Sturge M D, Manassen A, Cohen E and Pfeiffer L N 1996 *Solid State Commun.* **97** 741
[67] Siviniant J, Scalbert D, Kavokin A V, Coquillat D and Lascary J-P 1999 *Phys. Rev.* B **59** 1602
[68] Kossacki P, Ciulin V, Cibert J, Kutrowski M, Maslana W, Ferrand D, Tatarenko S, Wojtowicz T, Deveaud B and Gaj J A 2002 *Proc. Int. Conf. on Physics of Semiconductors (Edinburgh, 2002) (Inst. Phys. Conf. Ser. 171)* ed A R Long and J H Davies
[69] Vina L 1999 *J. Phys.: Condens. Matter* **11** 5929 and references therein
[70] Vinattieri A, Shah J, Damen T C, Kim D S, Pfeiffer L N, Maialle M Z and Sham L J 1994 *Phys. Rev.* B **50** 10868
[71] Kossacki P, Ciulin V, Kutrowski M, Ganière J-D, Wojtowicz T and Deveaud B 2003 at press
[72] Paganotto N, Siviniant J, Coquillat D, Scalbert D, Lascary J-P and Kavokin A V 1998 *Phys. Rev.* B **58** 4082
[73] Dacal L C O, Ferreira R, Bastard G and Brum J A 2002 *Phys. Rev.* B **65** 115325
[74] Sanvitto D, Pulizzi F, Shields A J, Christianen P C M, Holmes S N, Simmons M Y, Ritchie D A, Maan J C and Pepper M 2001 *Science* **294** 837
[75] Yoon H W, Sturge M D, Ron A and Pfeiffer L N 1997 *J. Lumin.* **72** 302
[76] Płochocka P, Kossacki P, Maślana W, Cibert J, Tatarenko S, Radzewicz C and Gaj J A 2003 at press